PERGAMON

International Journal of Solids and Structures 39 (2002) 3217–3231

INTERNATIONAL JOURNAL OF SOLIDS and STRUCTURES

www.elsevier.com/locate/ijsolstr

Mechanisms of stress transfer and interface integrity in carbon/epoxy composites under compression loading Part I: Experimental investigation

S. Goutianos [a,b], T. Peijs [b,c], C. Galiotis [a,b,*]

[a] *Institute of Chemical Engineering and High Temperature Chemical Processes Foundation of Research and Technology—Hellas, P.O. Box 1414, Patras 265 00, Greece*

[b] *Materials Department, Queen Mary University of London Mile End Road, London E1 4NS, UK*

[c] *Eindhoven Polymer Laboratories, Eindhoven University of Technology, P.O. Box 513, 5600 MB Eindhoven, The Netherlands*

Received 29 June 2001; received in revised form 14 February 2002

Abstract

Raman spectroscopy is used to get an insight into the microstructural aspects of the compressional behavior of carbon fiber composites. This is done by a comparative assessment of the stress transfer efficiency in tension and compression in single-fiber discontinuous model geometries. It was found that axial stress is transferred in the fiber through the generation of shear stresses at the interface for both tension and compression loading. Experimental evidence is presented to verify that the values of the maximum interfacial shear stress that the system sustains is a function of the applied strain and independent of the type of loading. However, compressive failure is quite different as fiber fragments remain in contact, thus can still bear load. © 2002 Published by Elsevier Science Ltd.

Keywords: Carbon fibers; Compression; Tension; Fiber/matrix interface; Raman spectroscopy; Composites

1. Introduction

Compressive failure is a design limiting feature of composite materials since the compressive strengths are often less than 60% of their respective tensile strengths (Budiansky and Fleck, 1991). Early investigations associated compressive failure with a fiber buckling process in an elastic matrix (Rosen, 1965). However, predictions were 3–4 times higher than the measured values, even when the initial assumptions were extended to account i.e. for non-linear matrix constitutive behavior. Argon (1972) and later Budiansky (1983) recognized the importance of initial fiber waviness or misalignment (although its quantification in composites is problematic) and that of (matrix or composite) shear yield strength as the main factors

* Corresponding author.
E-mail address: c.galiotis@iceht.forth.gr (C. Galiotis).

0020-7683/02/$ - see front matter © 2002 Published by Elsevier Science Ltd.
PII: S0020-7683(02)00240-8

controlling compressive strength. Failure is considered as a plastic microbuckling process (kinking) and a number of analytical models have been proposed for the prediction of the composites compressive strength. Usually the compressive strength, σ_u^c, is given as a function of initial fiber misalignment and matrix or composite shear yield strength (e.g. Christensen and DeTeresa, 1997; Fleck et al., 1995):

$$\sigma_u^c = \frac{G_{LT}^c}{1 + \frac{\phi_0}{\gamma_y^c}} \tag{1}$$

where G_{LT}^c is the composite shear modulus, ϕ_0 is the initial fiber misalignment and γ_y^c is the composite shear yield strain.

This equation predicts realistic compressive strengths, which are significantly lower than Rosen's results (Soutis and Curtis, 2000; Soutis et al., 2000). However, as mentioned by Schapery (1995) these analyses fall short of capturing many characteristic compressive features observed experimentally. Also these analyses do not really predict the onset of kinking which is presumed to pre-exist. A notable exception is the work of Kyriakides et al. (1995) who predicted kink band formation by growth of fiber waviness using a two-dimensional finite element model (initial fiber waviness was assumed). However, there are still questions regarding kink band formation and kink band broadening (Moran et al., 1995; Vogler and Kyriakides, 1999). Another issue that has to be verified is whether the fiber/matrix interface affects composite compressive strength as found by Madhukar and Drzal (1992). Other parameters that may have to be taken into account are the effects of free surfaces, stacking sequence, thickness of resin-rich regions between plies etc. (Guyn et al., 1992).

As it can be shown by Eq. (1), ϕ_0 has a large degrading effect on the composite strength. In literature the values given for ϕ_0 are usually 2–3° and the predicted compressive strengths (Eq. (1)) agree well with the experimental data. However, Creighton and Clyne (2000) observed kink band formation also in composites produced by pultrusion ($\phi_0 < 1°$). They suggested that initial microbuckling failure is triggered by fiber crushing mechanism which is contrary to the plastic microbuckling process mentioned above. In an earlier work, Kozey (1993) also suggested that kinking failure in a composite may be initiated by the compressive failure of fibers themselves and consequent formation of regions of instability in the composite. Andrews et al. (1998) reported that the compressive deformation of aramid fibers in pultruded rods is almost identical to the deformation of the individual aramid fibers. On the other hand, they observed that the compressive strength of the aramid fibers in the rods appears to be significantly lower than the compressive strength of the individual aramid fibers. This is attributed to possible co-operative compressive failure through kink band formation (Andrews et al., 1998). An alternative explanation for the non-linear response of composites consisting of highly anisotropic fibers such as carbon or aramid, is that the fibers themselves show a non-linear response in compression and soften at higher strains (Melanitis et al., 1994). Melanitis et al. (1994) observed that the stress–strain curves of glass fiber composites in tension and compression are fairly linear up to high values of applied strains and this reflects the behavior of the glass fibers themselves. However, significant non-linear effects are observed in carbon and kevlar composites and are directly associated to the mechanical behavior of the fibers themselves (Vlattas and Galiotis, 1993; Piggott and Harris, 1980).

As it becomes evident from the above, the compressive behavior of composites is still poorly understood (Jelf and Fleck, 1992). The complexity of the problem stems mainly from the variable failure modes observed and the behavior of fibers themselves. Hence any attempt to derive analytical expressions requires a full quantification of the various parameters such as the fiber misalignment, the matrix (or composite) shear yield strength, the fiber compressive yield strength and modulus, as well as, the effect of the fiber/matrix interface. The aim of this work is to get an insight into the microstructural aspects of compressional behavior in simple single-fiber model geometries so as to examine the stress transfer efficiency (interface) independent of all the other parameters which will be examined in the future. In order to highlight the

special features of the compressive behavior, an identical system is examined in tension as well. During loading of the model composites, the fiber stress or strain distribution along the fiber fragments is derived through the Raman spectrum of the carbon fiber and its stress or strain dependence. The corresponding interfacial shear stress (τ_{rz}) distribution is evaluated by means of a balance of forces argument, given by:

$$\frac{\partial\langle\sigma_{zz}^{f}\rangle}{\partial z} = -\frac{2\tau_{rz}}{r_f} \tag{2}$$

where $\langle\sigma_{zz}^{f}\rangle$ is the average axial stress in the fiber and r_f is the fiber radius. Such microcomposites, in spite of the unrealistic stress state, are valuable in gaining an understanding of the controlling damage mechanisms. However, although single fiber tests seem, at first sight, to be ideal to investigate the role of the constituents (fiber and matrix) and fiber/matrix interface on the overall composite behavior, there is a lot of criticism regarding these tests (Piggott, 1997), i.e. different microtests are unable to provide similar answers for the level of interface adhesion of a given composite system. Thus, care should be taken in the interpretation of the experimental data and a comparative assessment between tension and compression may lead to more accurate conclusions rather than those based on the absolute values of interfacial shear strength.

2. Experimental

2.1. Materials and specimen preparation

Surface treated high-modulus carbon fibers (M40-40B) were used as reinforcement material, the mechanical properties of which are given in Table 1. Fibers had an effective diameter of 6.6 μm and were embedded in a two part system Epikote 828/Ankamine 1618 (Shell). The resin (Epikote 828) and the hardener (Ankamine 1618) were mixed at 50 °C at a ratio 5:3 and degassed for 15 min under full vacuum.

Two different specimen geometries were employed; namely a dogbone geometry used in tension experiments and a prism geometry for the case of compression tests, see Fig. 1. The prism length is twice its width/thickness to avoid buckling according to ASTM D 695 standards. To produce the short-fiber specimens in both cases the resin, after being degassed, was first poured into a silicon rubber mold (dogbone specimens) or Teflon mold (compression specimens). Then the fibers were carefully placed and aligned on

Table 1
Mechanical properties of fiber and resin

Mechanical paramaters	M40-40B carbon fiber	Epoxy matrix
E_L^t (GPa)	390	1.5
E_L^C (GPa)	–	2.0
E_T^t (GPa)	14	–
E_{LT}^t (GPa)	20	0.58
ν_{LT}	0.20	0.3
ν_{TT}	0.25	–
σ_y^c (MPa)	–	55
σ_y^t (MPa)	–	35

E: Young's modulus, G: shear modulus, ν: Poisson's ratio, σ_y: yield stress, L: longitudinal direction, T: transverse direction, t: tension, c: compression.

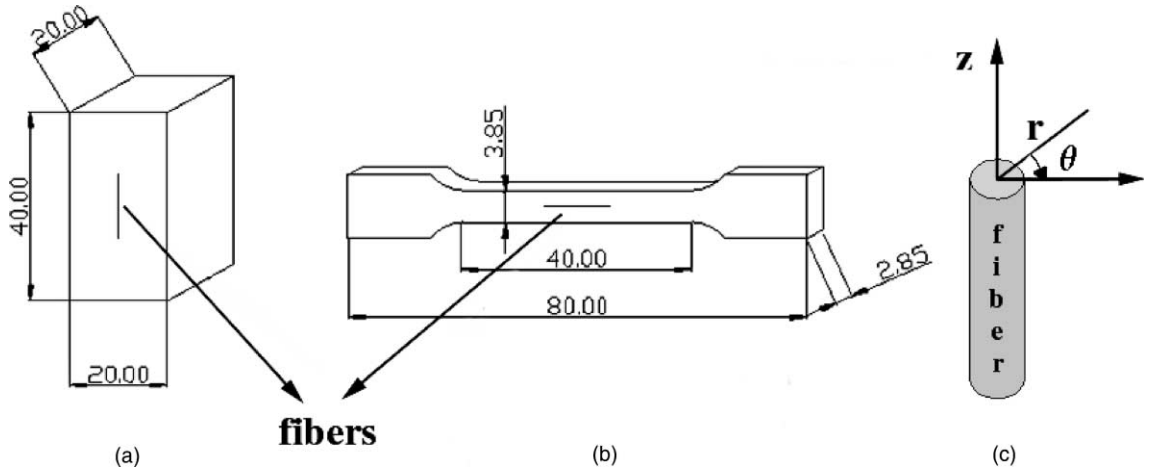

Fig. 1. Geometry of single-fiber specimens: (a) prism geometry for compression tests, (b) dogbone geometry for tension tests (all dimensions in mm) and (c) cylindrical coordinate system.

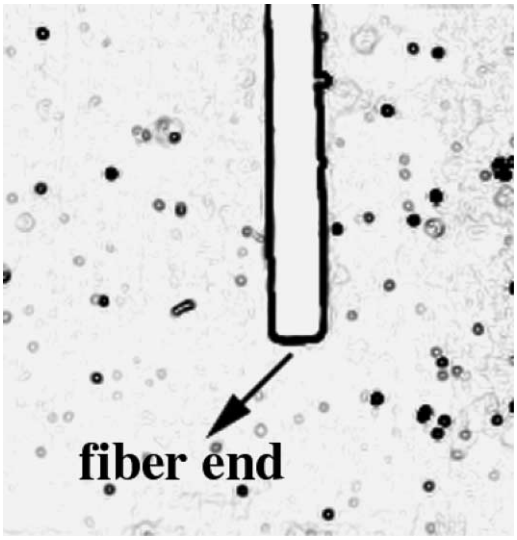

Fig. 2. Micrograph of a section of the fibre near its end. The fiber diameter is approximately 6.6 μm.

top and at approximately the mid-width of the specimen. Care was taken to embed the fibers at a small distance away from the surface. The composite coupons were cured at room temperature for one week; a low curing temperature was selected in order to eliminate the development of residual stresses on the embedded fibers. Prior to mechanical testing, the residual stresses on the embedded fibers were measured; specimens in which the fiber residual stresses were large or the fiber ends were distorted were discarded (Fig. 2 depicts a typical fiber end). The fiber lengths varied from $\sim$1.8 to $\sim$7.0 mm (the length of the short fibers was not controlled). However, as long as fiber length is greater than the ineffective or transfer length, there is no influence on the results obtained.

2.2. Specimen testing and Raman spectra acquisition

Raman spectra were taken with a remote Raman microprobe developed by Paipetis et al. (1996). The laser used was a 514.5 nm argon ion laser. An incident power of ~1.2 mW and an exposure time of 60 s were chosen in order to avoid fiber overheating. The spectral characteristics, i.e. peak positions were derived by fitting the raw data with Lorentzian distribution functions.

The shift of the Raman wave number of the carbon fibers upon the application of a tensile or compressive strain was measured with the cantilever beam test (Vlattas and Galiotis, 1993). This was done by attaching individual filaments on the top surface of a specially made cantilever beam which can be flexed up or down subjecting the fibers to compression or tension, respectively. Substantial matrix Raman activity is observed in the 500–1700 cm^{-1}region, moreover with the application of a compressive load, Raman peak shifts to higher wave number values, that is into the matrix Raman peak. However, at high wave numbers the matrix material exhibits very little Raman activity (van den Heuvel et al., 1998) therefore the second order peak of the carbon fiber at 2760 cm^{-1} was employed for fiber strain measurements. The Raman wave number shift versus strain is shown in Fig. 3. The experimental data were fitted with a 6th order polynomial of the form:

$$p_1\epsilon + p_2\epsilon^2 + p_3\epsilon^3 + p_4\epsilon^4 + p_5\epsilon^5 + p_6\epsilon^6 = \Delta v \tag{3}$$

where p_i are constants and Δv is the wave number shift of the Raman peak due to strain ϵ. Eq. (3) imposes continuity between tension and compression and satisfies the natural condition:

$$\Delta v = 0 \quad \text{for } \epsilon = 0 \tag{4}$$

A 6th order polynomial was necessary in order to accurate fit the experimental data and extrapolate them. The indicative strain sensitivity at zero strain is $p_1 = -20$ $cm^{-1}/\%$. Alternatively, the experimental data of Fig. 3 can be fitted with cubic splines (e.g. Chohan and Galiotis, 1996; Galiotis et al., 1999). Since the experimental data are quite smooth, a polynomial fitting was more preferable (in spite of its high degree) than cubic splines since polynomials are simpler to use and the interpolation function is known.

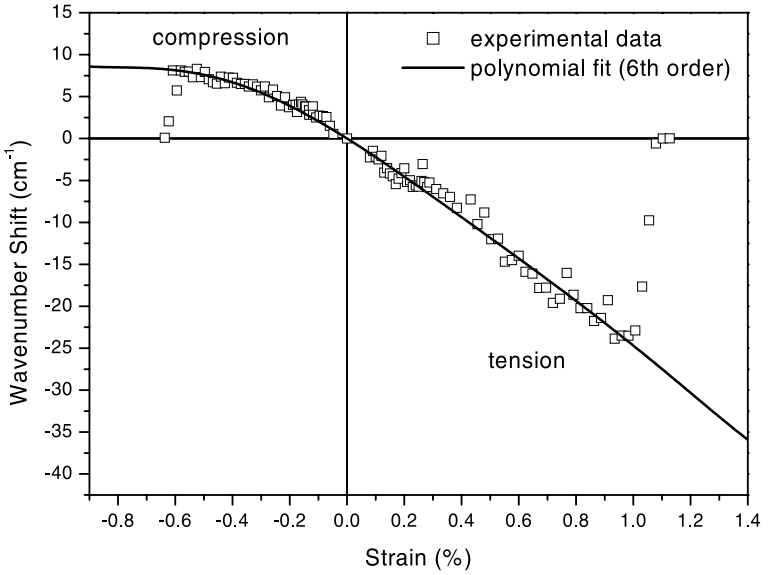

Fig. 3. Raman wave number shift versus strain for the M40-40B carbon.

As it can be seen in Fig. 3 the M40-40B carbon fiber fails at a strain of approximately 1% in tension whereas its compressive failure strain is about −0.6%. The calibration curve is in very good agreement with the data given in Narayanan and Schadler (1999b). As shown, even high modulus carbon fibers display a non-linear behavior in compression, the linear part extends up to a strain of −0.35% approximately. In addition it can be observed that the compressive failure strain of the carbon fibers is significantly lower than the tensile failure strain, which is in contrast with the results reported by Vincon et al. (1998). It is worth adding here that the wave number vs. axial stress curve has been found to be linear as these fibers can be considered as equal-stress bodies with crystallites connected in series within a narrow orientation distribution. The corresponding value of the slope of the wave number vs. axial stress line has been measured to be $-3.0\ \mathrm{cm}^{-1}$/GPa (Chohan and Galiotis, 1996) for the first order region and estimated to be $-5.0\ \mathrm{cm}^{-1}$/GPa for the second order region.

The short-fiber specimens were mounted on a Hounsfield universal testing machine and strained at distinct strain levels up to ∼−0.9% for the case of compression and up to ∼1.25% in the case of tension. The applied tensile strain rate, used for the transition form one strain level to the next one, was $2.1 \times 10^{-5}\ \mathrm{s}^{-1}$, whereas the compressive strain rate was $4.2 \times 10^{-5}\ \mathrm{s}^{-1}$. Point-to-point Raman measurements were taken along the fiber at each strain level. Laser Raman sampling was carried out in steps of 2 μm at the vicinity of the fiber ends (from 0 to 100 μm) or fiber breaks, then in steps of 5 μm (from 100 to 300 μm) and then in steps of 10/20 μm until the middle of the fiber. The above protocol is necessary to ensure detailed mapping of stress near the discontinuity where the first derivative of the stress transfer function reaches a maximum value. The applied strain on the specimens was also monitored by a strain gauge of gauge factor 2.09 attached to the resin surface. In the case of compressive loading two strain gauges were used, attached on opposite sides to detect any possible macrobuckling of the specimens.

2.3. Analysis of the experimental data

The mapping of the stress or strain distribution along an embedded fiber allows the determination of all the important interfacial parameters (e.g. transfer length, mode of failure, interfacial shear stress etc.). It should be mentioned however that all micromechanical tests are actually indirect methods to assess the parameters mentioned above. In this case, someone has to resort to approximate analytical solutions such as is attempted by conventional micromechanical analyses (e.g. Cox, 1952; Piggott, 1978). However, a careful examinations of the existing stress transfer models reveals that they contain adjustable parameters that can be set to a certain value so that they match the experimental data. Moreover, the use of these models (which are derived through certain approximations) requires the a priori choice of the failure mode observed (e.g. matrix yielding or interfacial debonding). More importantly, there are no stress transfer models available in the literature, which could be applied to describe the fiber stress in the vicinity of a compressive fiber break. On the other hand, a direct fit procedure of the experimental data does not require any assumption about the materials behavior or failure mode present in the single-fiber model composites. Thus, the information that can be extracted is subjected only to the numerical error of the technique. To facilitate data manipulation polynomials are fitted to the raw fiber stress/strain values. However, if a function is to be approximated on a larger interval the degree of the approximating polynomial may have to be unacceptably large. The alternative solution is the use of spline polynomial functions such as the B-cubic splines. Like most numerical methods, spline interpolation requires an initial solution as an input, which is the most arbitrary part of the analysis.

A Matlab program was made to fit the experimental data with B-cubic splines. The program required as input the number of cubic polynomial functions used to fit the data. The knots introduced in this way were equispaced, and, then, it was possible to move the knots so that the best least-square approximation achieved. The most trivial part of the analysis is the initial number of polynomials used. Clearly, a small number of polynomials affects detrimentally the best fit, whereas a large number of polynomials is affected

by the presence of noise of the Raman measurements. The important parameter here is to define the minimum number of polynomials needed to describe sufficiently the stress transfer problem. We have fitted the data at every strain level using a range of polynomials from 2 up to 40 (depending on the applied strain). Then by comparing the stress and ISS profiles of different applied strain levels we were able to choose quite safely the number of knots. Simple but physically sound criteria were used, i.e. as the applied strain increases the necessary number of knots to describe the phenomenon should also increase (or at least be equal to the number of knots used in the immediate previous strain step) since the stress field becomes more complex. When at a distinct strain level an interfacial failure is predicted then at a higher strain interfacial failure should also occur.

The selection of B-cubic splines imposes interfacial shear stress continuity along the fiber length irrespective of the local interface integrity. This seems to be a more reasonable approach compared e.g. to Piggott (1978) or Nairn and Liu (1997) models in which ISS discontinuity occurs between a damaged and an intact interfaces.

3. Results

3.1. Compressive behavior

Figs. 4(a) and 5(a) depict the axial fiber stress along the length of a carbon fiber embedded in an epoxy matrix at different compressive strain levels. These graphs have been produced by converting the wave number shifts into values of axial stress using the wave number stress calibration factor mentioned above. In these graphs, there is the impression of significant amount of noise. However, this is mainly due to the small strains applied to the microcomposites in contrast with previous reported data. Moreover, the data scatter is not only due to the experiment; it is also due to the real material variations at the microscale of the experiment. Figs. 4(b) and 5(b) show the corresponding interfacial shear stresses. At these low applied compressive strains it was relatively easy to control the macroscopic matrix strain. That is creep effects were not present and this is well demonstrated in Figs. 4(a) and 5(b) where it can be observed that the fiber stress

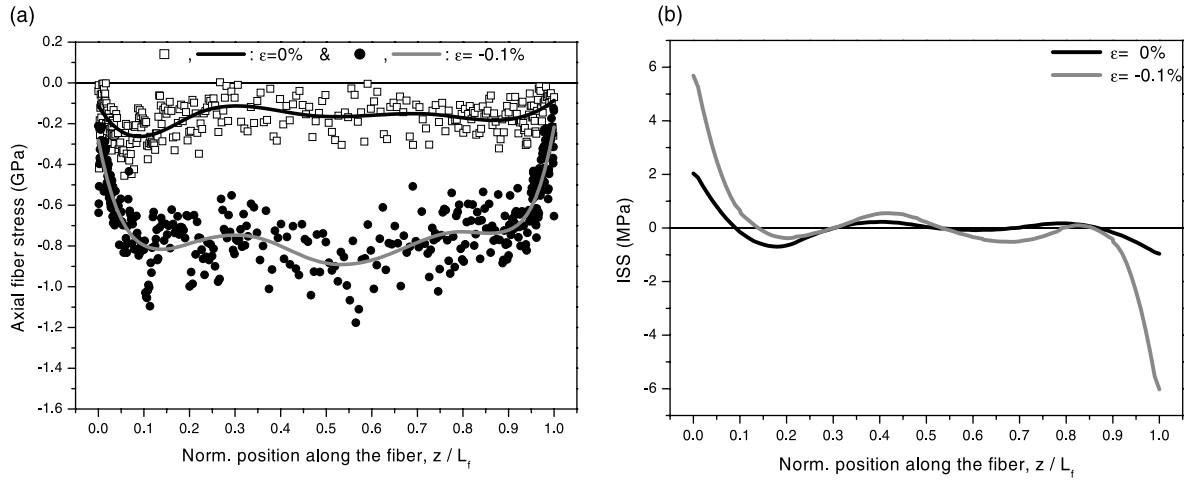

Fig. 4. (a) Axial fiber stress profile of an embedded fiber ($L_f = 3$ mm) in an epoxy matrix loaded at strains of 0% and −0.1% respectively. The open squares/solid circles correspond to experimental data whereas the solid lines represent the corresponding cubic spline fits. (b) Corresponding interfacial shear stresses.

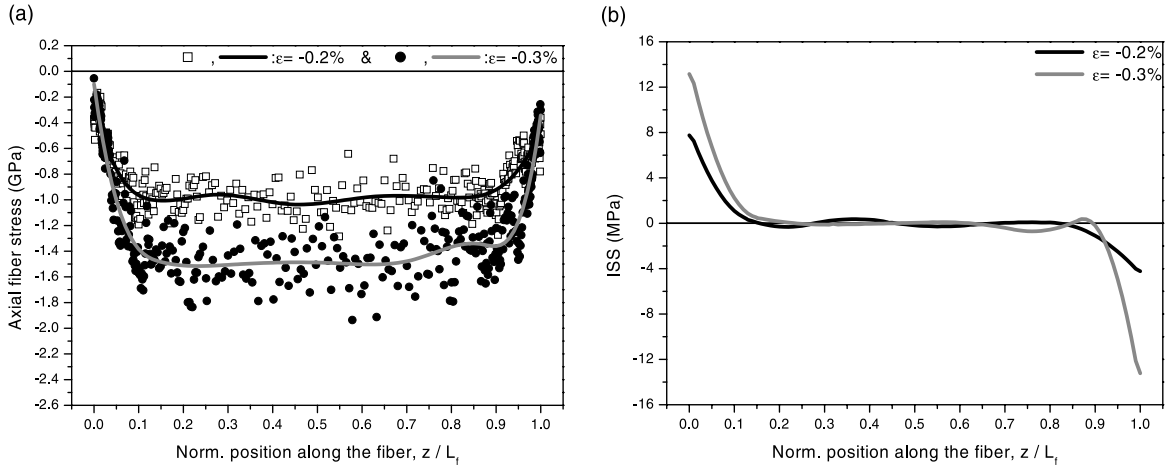

Fig. 5. (a) Axial fiber stress profile of an embedded fiber ($L_f = 3$ mm) in an epoxy matrix loaded at strains of −0.2% and −0.3% respectively. The open squares/solid circles correspond to experimental data whereas the solid lines represent the corresponding cubic spline fits. (b) Corresponding interfacial shear stresses.

profiles are almost perfectly symmetric. As it can be seen from Fig. 4(a), the fiber is relatively stress-free in the unstrained case, with the residual compressive stress being about −0.1 GPa. When the matrix strain (applied strain) increases, the fiber stress increases rapidly from the fiber ends to a plateau value along the middle of the fiber. The stress is transferred from the fiber ends through shear at the interface as in the case of tensile loading. A value of ineffective or transfer length of the order of 350 μm is observed ($L_f = 3$ mm). In the unstrained case the axial stress in the fiber ends is ∼−0.015 and −0.07 GPa, respectively. At an applied strain −0.1%, the axial fiber stress at the fiber ends increases to ∼−0.20 and −0.14 GPa, for the left and right end, respectively. However further increase of the applied strain has almost no effect on the left fiber end (σ_{zz} fluctuates about −0.20 GPa) while at the right fiber end the axial stress reaches a value of about −0.30 GPa and then remains relatively constant. No interfacial failure is observed (see Figs. 4(b) and 5(b)) for a strain lower than that required for fiber failure. Finally, it is worth noting that there is no indication from Fig. 4(a) of any direct load transmission through the fiber ends. Similar results (stress transfer through shear activated mechanisms) were obtained by Narayanan and Schadler (1999b) and Mehan and Schadler (2000).

3.2. Compressive failure

In order to study the post-failure stress transfer mechanisms, the specimens were compressed to sufficiently high strain levels to induce multiple fiber fracture. Fig. 6(a) depicts the stress profile in a fiber embedded in an epoxy matrix when the microcomposite is loaded at average strains equal to −0.86%.

Similarly to the results presented above, up to strains of about −0.35% no fiber failure occurs, and the quality of the interface seems to be unchanged. However, at an applied strain of ∼−0.6% multiple fiber fracture is observed. This strain level is equal to the fiber compressive failure strain as it can be seen from Fig. 3. Further increase of the applied strain results almost in complete fiber fragmentation (see Fig. 6(a)).

It can be seen from Fig. 6(a) that the cubic spline fit fails to describe the experimental data in the neighborhood of fiber breaks. In order to do so, we should significantly increase the number of knots used but this obviously would affect the best of fit in the fiber ends regions. Moreover, as it will be discussed later, it is meaningless to fit the experimental data at the vicinity of compressive fiber breaks. Fig. 7 depicts a

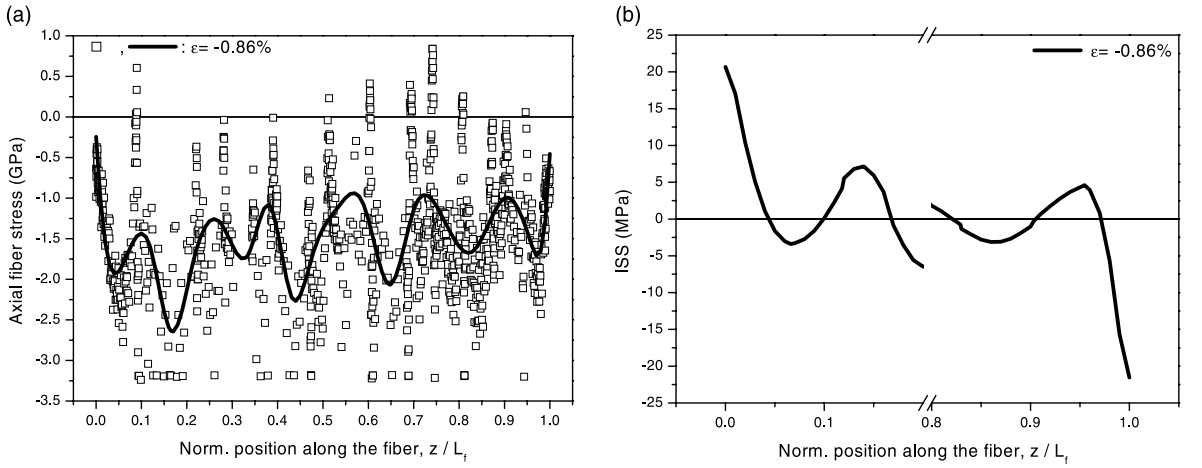

Fig. 6. (a) Axial fiber stress profile of an embedded fiber ($L_f = 6.3$ mm) in an epoxy matrix loaded at a strain of -0.86%. The open squares correspond to experimental data whereas the solid line represents the corresponding cubic spline fit. (b) Corresponding interfacial shear stresses.

micrograph of a typical shear compressive fiber break observed in all the experiments performed. It can be easily seen that the broken ends slide past each other and therefore compressive stresses can be transmitted as the fiber fragments remain in contact. This is the reason for the very low compressive ineffective length ~40–80 μm (Fig. 6(a)) compared to the tensile ineffective length (450–500 μm). Similarly, Amer and Schadler (1997) found that at a strain of -0.6% the compressive average fragment length is about 85 ± 10 μm for a M40/epoxy system.

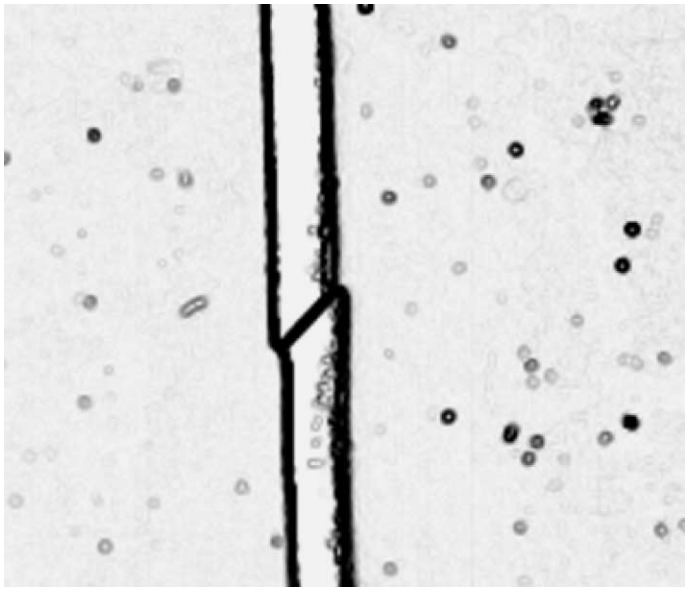

Fig. 7. Micrograph of a typical compressive fiber break indicating predominant shear failure. The fiber diameter is approximately 6.6 μm.

Concerning the stress transfer from the fiber end discontinuities it can be observed that even at strains, exceeding the compressive failure strain of the fiber, no substantial interfacial damage occurs. Fig. 6(a) clearly shows that no debonding or yielding occurs in these regions within experimental error.

3.3. Tensile behavior

Fig. 8(a) shows the stress profile of a fiber loaded in tension at applied strains of 0%, 0.2% and 0.4%. As can be seen, the residual stress fluctuates around zero (0% applied strain) although there is an indication of the presence of compressive stresses particularly around the right fiber end. At an applied strain of 0.2% the stress builds from zero at the left fiber end to a maximum value of about 800 MPa and from −200 to 600 MPa for the right half of the fiber. At an applied strain of 0.4% and at a normalized distance of 0.3–0.4 (550–700 μm) from the left fiber end, an unexpected decrease of the fiber stress is observed which might be associated with a fiber flaw and/or the onset of fiber failure. The stress distortion of spread of ~200 MPa is also observed at applied strains of 0.6% and 0.8%. It is interesting to note that at an applied strain of 1.25% (see Fig. 9(a)) fiber fracture occurs at the locus of the observed fiber stress perturbation. The fiber stress at break location is equal to the initial residual stress within the experimental and numerical errors. The ineffective or transfer length (L_t) is of the order of 450–500 μm (see Fig. 9(a)).

Since a kind of interfacial damage pre-exist in the left fiber end, only the right fiber end will be used to assess the interfacial state during tensile loading. The ISS increases from ~1.5 MPa at zero applied strain (Fig. 8(b)) to ~20 MPa at an applied strain of 0.8%. At an applied strain of 1.1% interfacial damage occurs (see Fig. 9(b)), and the ISS profile displays a "knee" which is located 100 μm from the fiber end. The maximum ISS value is somewhat less than 20 MPa. The existence of interfacial damage can also be easily identified from the stress data (see Fig. 9(a)). The growth of the interfacial damage zone with applied strain is also very well depicted in Fig. 9(a) and (b). The maximum ISS value observed at an applied strain of 1.25% is located 185 μm from the fiber end. The maximum ISS values observed around the fiber break or the left fiber end (all <20 MPa) leads us to the conclusion that the interfacial shear strength of the composite system examined is ~20 MPa. There are discrepancies between the ISS values obtained at the left and right fiber ends which are within the accuracy of the measurements performed (±5 MPa). It is worth

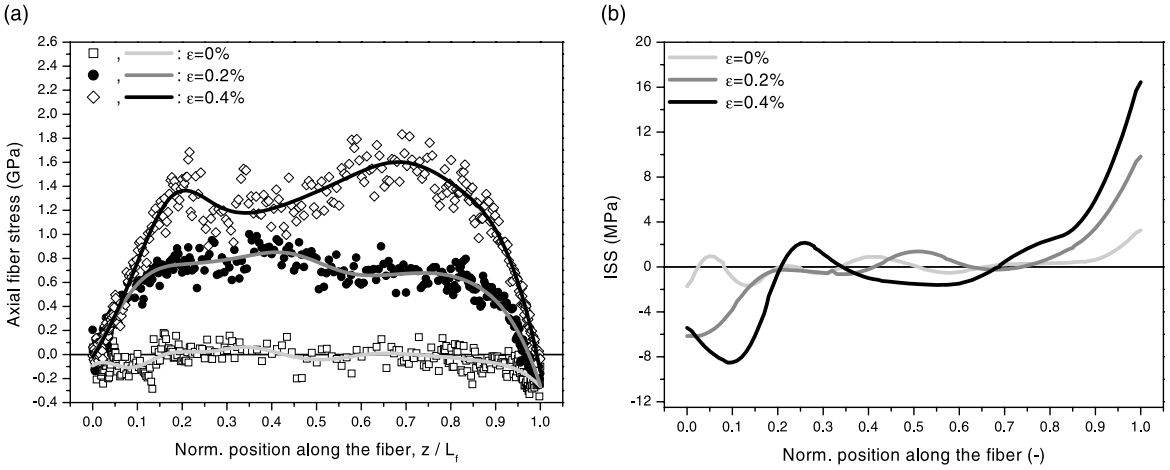

Fig. 8. (a) Axial fiber stress profile of an embedded fiber ($L_f = 1.8$ mm) in an epoxy matrix loaded at strains of 0%, 0.2% and 0.4% respectively. The open diamonds/squares/solid circles correspond to experimental data whereas the solid lines represent the corresponding cubic spline fits. (b) Corresponding interfacial shear stresses.

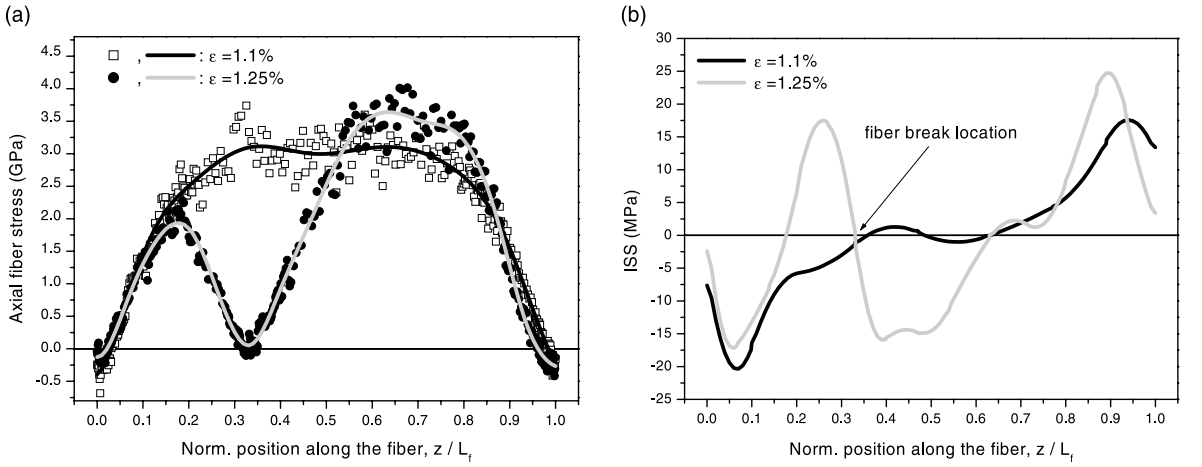

Fig. 9. (a) Axial fiber stress profile of an embedded fiber ($L_f = 1.8$ mm) in an epoxy matrix loaded at strains of 1.1% and 1.25% respectively. The open circles/squares correspond to experimental data whereas the solid lines represent the corresponding cubic spline fits. (b) Corresponding interfacial shear stresses.

mentioning here that the shear yield stress of the resin has been estimated to be 31.7 MPa by employing the von Mises criterion to the compressive yield stress (Table 1). At the right side of the fiber break (Fig. 9(b)) shear yielding at the interface can also be identified. Finally, another important conclusion is that fiber/matrix debonding does not occur even at strains of 1.25% for this fiber/matrix combination.

4. Discussion

4.1. Compressive failure

The stress build-up emanating from a compressive fiber break (Fig. 6(a)) is quite different from that in tension (see Fig. 9(a)). To start with, the fiber stress at a compressive fiber break location does not necessarily drop to zero or to the initial residual stress. In addition, the rate of stress transfer from a fiber break is extremely high and therefore the corresponding transfer (ineffective) length is extremely small when compared to that in tension (Fig. 9(a)). As mentioned earlier, compressive failure for the high-modulus fiber/epoxy system examined here leads to fiber ends sliding past each other. By further loading of the system, stress is transferred in the fiber not only by interfacial shear but also by fiber–fiber contact at the compressive failure location. Unlike previously reported work (Narayanan and Schadler, 1999b; Mehan and Schadler, 2000), an attempt has been made here to distinguish between the two types of stress transfer so as to assess the relative importance of interfacial adhesion in compression. As can be seen in Fig. 6(a), the rate of stress transfer from the left or right fiber ends is comparable with that observed in tension from a fiber break (or a fiber end) since the prevailing stress-transfer mechanism at those locations is pure interfacial shear. By limiting the true interfacial shear stress measurements in the case of compression to the fiber ends reasonable values of maximum ISS of the order of 25 MPa have been obtained. In fact, the ISS calculations from compressive failures in the middle of the fiber (Fig. 6(b)) have been omitted since the balance of forces argument is not valid there. It is worth adding that the derivation of Eq. (2) is based on axisymmetric elasticity theory, however when the fiber fails in compression and the broken fiber fragments slide past each other the symmetry rule changes and, therefore, the use of Eq. (2) can lead to erroneous

results. Narayanan and Schadler (1999a) in their earlier work have employed Eq. (2) to calculate the ISS in the case of compressive fiber breaks and they reported ISS values in excess of 150 MPa (Amer and Schadler, 1997) and even 300 MPa (Amer and Schadler, 1997) for similar fiber/matrix systems. Since these values were unacceptably high, an attempt was made (Narayanan and Schadler, 1999a) to modify the balance of forces argument to account for the post-failure geometric configuration as given below:

$$\frac{\partial\langle\sigma_{zz}^{\mathrm{f}}\rangle}{\partial z} = -\frac{2\tau_{rz}}{r_{\mathrm{f}}}\sin\phi \tag{5}$$

where ϕ is the bending angle (see Narayanan and Schadler, 1999a) determined to be approximately 8°. Based on the above formula the ISS value is reduced by a factor of ~7 and therefore a "corrected" ISS value of approximately 51 MPa was obtained. The latter value is still too high for a high-modulus carbon fiber/epoxy system presumably due to the simplistic arguments employed for its derivation. As stated by same authors (Narayanan and Schadler, 1999a), a more rigorous analysis is needed to estimate accurately the interfacial shear stress in the neighborhood of compressive fiber breaks. At the moment, the mapping of the ISS distribution from the fiber ends is the only accurate method available for assessing the fiber/matrix adhesion under compressive loading.

Another interesting feature observed at the loci of fiber failure in compression is the fact that the stress fluctuates around zero and, in some cases (Fig. 6(a)), it reaches tensile values. This is again due to the deformation and bending of fibers at the point of shear failure which depending on the laser Raman sampling direction, can be also tensile. These results are in distinct contrast with those reported by Wood et al. (1995) for which the fiber strain profiles were completely unaffected by the fragmentation process. However, the photoelastic fringes produced by the fiber failures (see Wood et al., 1994) clearly showed that stress perturbations did occur even in that case. It must also be noted that Wood et al. (1995) identified a bulging mode of failure in compression for their high modulus pitch-derived fibers in contrast with the shear mode of failure observed here. In an earlier work, Hawthorne and Teghtsoonian (1975) also observed compression induced shear failure in carbon fiber produced from pitch, rayon and polyacrolonitrile. Prior to fracture hair-like cracks in the fiber surface were observed. They concluded that as fiber anisotropy increases the tendency is away from a single catastrophic shear-like failure to what is often a series of fine, partial microcracks. They suggested that for high modulus fibers microcracking may initiate as a buckling of microfibrils of well-ordered graphite crystallites. More recently, Boll et al. (1990) found that intermediate modulus fibers embedded in an epoxy matrix fail by shear. Compression failure initiates as a microcrack, which then propagates as a shear failure. Subsequent post failure damage may take a variety of forms such as fiber crushing, longitudinal splitting, bifurcation of shear fracture etc. Finally, Melanitis et al. (1994) have performed systematic studies on PAN based carbon fibers of various moduli and observed that bulging is only present in low modulus fibers and as the modulus increases shear failure clearly dominates.

4.2. Comparison of compressive versus tensile behavior

In Fig. 10 the far-field fiber strain vs. the applied strain for both loading conditions (tension and compression) has been plotted. At low strains an approximately linear relationship between fiber strain and applied strain (matrix strain) is obtained for both types of loading. However, for strains higher than 0.8% in tension and −0.35% in compression a deviation from linearity is observed. Based on earlier arguments, it is clear that the cause of the nonlinear behavior is different in the two cases examined. In tension, the gradual deviation from linearity prior to fiber fracture within the range of 0.8–1.1% strain is attributed to the onset of matrix plasticity and hence the reduction of its shear modulus at high strains (this early onset of matrix plasticity is due to the cold curing of the resin). In compression, the significant reduction of the strain sustained by the fiber is due to the multiple fiber failure that is observed at strains lower than −0.56%.

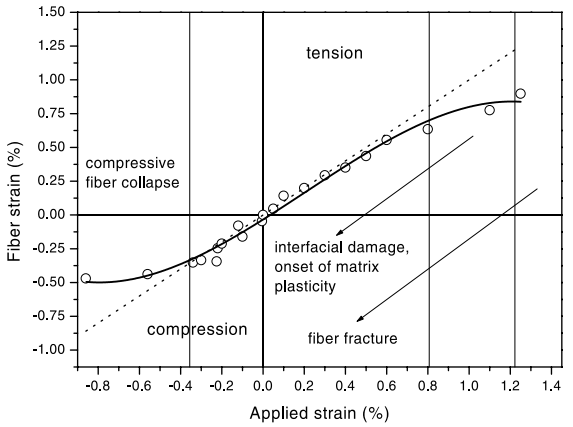

Fig. 10. Axial far-field fiber strain ($\epsilon_{\text{fiber}} = \epsilon_{\text{measured}} - \epsilon_{\text{residual}}$) vs. applied strain. The dotted line represents the 1:1 relation between the applied strain and the far-field fiber strain, whereas the solid line represents a third degree polynomial fit of the experimental data (◯).

In terms of failure characteristics, it has been recognized in the earlier work of Rosen (1964) that composite tensile failure is governed by the statistical distribution of fiber flaws or imperfections. For example, as mentioned already, the fiber break observed in Fig. 9(a) might be associated with a fiber flaw. Another, observation is that the tensile fragment distribution is far from uniform i.e. see van den Heuvel et al. (1997) and Paipetis and Galiotis (1997). On the contrary it can be observed from Fig. 6(a) that the compressive fragmentation process exhibits a clear uniformity. This is an indication that compressive fracture is not governed primarily by a random flaw distribution as in the case of tensile loading. Boll et al. (1990) reached the same conclusion, by observing that for an AS4 fiber embedded in an epoxy matrix the compressive average fragment size was 0.18 mm. The size distribution was quite narrow and relatively symmetrical, whereas the average fragment length in tension was found to be around 0.40 mm and the distribution was highly skewed (see also Favre and Jacques, 1990). Hawthorne and Teghtsoonian (1975) examined numerous compression fractures and found only a few examples where fracture might possibly

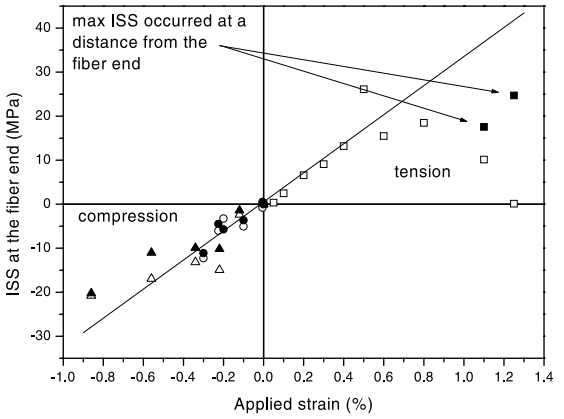

Fig. 11. Maximum ISS values ($\text{ISS}_{\max} = \text{ISS}^{\max}_{\text{measured}} - \text{ISS}^{\max}_{\epsilon=0\%}$) vs. applied strain. The different symbols in the left part (compression) of the graph correspond to different experiments, whereas the solid squares in the tensile section of graph represent measurements at a distance from the fiber ends. The solid line represents the linear fir of the experimental data for $-0.3\% < \epsilon < 0.3\%$.

have been associated with an observable flaw. Hence, it seems that the compressive carbon fiber failure may be determined by its microcrystalline structure rather than by random defects.

In Fig. 11 the maximum ISS values obtained at various levels of applied strain over both tension and compression regimes and for both fiber ends are presented. As seen, the max. ISS takes up similar values for a given applied strain regardless of the direction of loading. In fact, deviations from linearity are observed at strains higher than 0.6% for both regimes, which indicate that (a) the interface holds well in compression in spite of the shear failure of the fiber which occurs at lower strains and (b) the origin of the slight drop of max. ISS should be attributed to the reduction of shear modulus and not to interface failure since the maximum value is obtained at the fiber ends. Further increase of the input strain in tension shifts the maximum towards the middle of the fiber, due to the onset of interface failure followed by possible debonding or matrix cracking as the ISS at the fiber end drops to zero (Fig. 11). It is interesting to note that the new maxima generally follow the overall curve indicating further gradual drop of shear modulus with increasing strain.

5. Conclusions

A detailed investigation of the compressive behavior of high-modulus carbon fibers embedded in an epoxy matrix was performed by means of a comparative assessment of stress transfer efficiency in tension and compression. It was shown that:

1. The mapping of the ISS distribution from the fiber ends is the only accurate method available for assessing the fiber/matrix adhesion under compressive loading. The maximum values of ISS obtained in both cases (tension and compression) was of the order of 25 MPa.
2. At low strains an approximately linear relationship between fiber strain and applied strain (matrix strain) is obtained for both types of loading. At high compressive strains the deviation from linearity is due to the multiple fiber failure. On the other hand, the deviation from linearity in tension is related to the onset of matrix plasticity.
3. The stress build-up emanating from a compressive fiber break is quite different from that in tension. The fiber stress at a compressive fiber break location does not necessarily drop to zero or to the initial residual stress.
4. The rate of stress transfer from a fiber break is extremely high and therefore the corresponding transfer (ineffective) length is extremely small when compared to that in tension (8–16%).

References

Amer, M.S., Schadler, L.S., 1997. Stress concentration phenomenon in graphite/epoxy composites: tension/compression effects. Compos. Sci. Technol. 57, 1129–1137.

Andrews, M.C., Young, R.J., Mahy, J., Schaap, A.A., Grabandt, O., 1998. Compressive behavior of aramid fiber-reinforced pultruded rods. J. Compos. Mater. 32, 893–908.

Argon, A.S., 1972. Fracture of composites. In: Treatise of Material Science and Technology, vol. 1. Academic Press, New York, NY.

Boll, D.J., Jensen, R.M., Cordner, L., 1990. Compression behavior of single carbon filaments in an epoxy polymer. J. Compos. Mater. 24, 208–219.

Budiansky, B., 1983. Micromechanics. Comput. Struct. 16 (1–4), 3–12.

Budiansky, B., Fleck, N.A., 1991. Compressive failure of fibre composites. J. Mech. Phys. Solids 41 (1), 183–211.

Chohan, V., Galiotis, C., 1996. Interfacial measurements and fracture characteristics of 2d microcomposites using a remote laser raman microscopy. Composites Part A. 27, 881–888.

Christensen, R.M., DeTeresa, S.J., 1997. The kink band mechanism for the compressive failure of fiber composite materials. J. Appl. Mech. 64, 1–6.

Cox, H.L., 1952. The elasticity and strength of paper and other fibrous materials. British J. Appl. Phys. 3, 72–92.
Creighton, C.J., Clyne, T.W., 2000. The compressive strength of highly-aligned carbon/epoxy composites produced by pultrusion. Compos. Sci. Technol. 60, 525–533.
Favre, J.P., Jacques, D., 1990. Stress transfer in carbon fibre model composites. J. Mater. Sci. 25, 1373–1380.
Fleck, N.A., Deng, L., Budiansky, B., 1995. Prediction of kink width in compressed fiber composites. J. Appl. Mech. 62, 329–337.
Galiotis, C., Paipetis, A., Marston, C., 1999. Unification of fibre/matrix interfacial measurements with raman microscopy. J. Raman Spectrosc. 30, 899–912.
Guyn, E.G., Bradley, W.L., Ochoa, O., 1992. A parametric study of variables that affect fiber microbuckling initiation in composite laminates. Part 2: Experiments. J. Compos. Mater. 26 (11), 1617–1643.
Hawthorne, H.M., Teghtsoonian, E., 1975. Axial compression fracture in carbon fibres. J. Mater. Sci. 10, 41–51.
Jelf, P.M., Fleck, N.A., 1992. Compression failure mechanisms in unidirectional composites. J. Compos. Mater. 26 (18), 2706–2726.
Kozey, V.V., 1993. Fibre strength-dominated failure mode in unidirectional composites under compression. J. Mater. Sci. 12, 48–52.
Kyriakides, S., Arseculeratne, R., Perry, E.J., Liechti, K.M., 1995. On the compressive failure of fiber reinforced composites. Int. J. Solids Struct. 32 (6–7), 689–738.
Madhukar, M.S., Drzal, L.T., 1992. Fiber–matrix adhesion and its effect on composite mechanical properties. III. Longitudinal (0°) compressive properties of graphite/epoxy composites. J. Compos. Mater. 26 (3), 310–333.
Mehan, M.L., Schadler, L.S., 2000. Micromechanical behavior of short-fiber polymer composites. Compos. Sci. Technol. 60, 1013–1026.
Melanitis, N., Tetlow, P.L., Galiotis, C., Smith, S.B., 1994. Compressional behaviour of carbon fibres. J. Compos. Mater. 29, 786–799.
Moran, P.M., Liu, X.H., Shih, C.F., 1995. Kink band formation and band broadening in fiber composites under compressive loading. Acta Metall. Mater. 43 (8), 2943–2958.
Nairn, J.A., Liu, Y.C., 1997. Stress transfer into a fragmented anisotropic fiber through an imperfect interface. Int. J. Solids Struct. 34 (10), 1255–1281.
Narayanan, S., Schadler, L.S., 1999a. Assessment of strains along fiber surface features in graphite/epoxy composites loaded in compression. Compos. Sci. Technol. 59, 1589–1596.
Narayanan, S., Schadler, L.S., 1999b. Mechanisms of kink-band formation in graphite/epoxy composites: a micromechanical experimental study. Compos. Sci. Technol. 59, 2201–2213.
Paipetis, A., Galiotis, C., 1997. A study of the stress-transfer characteristics in model composites as a function of material processing fibre sizing and temperature of the environment. Compos. Sci. Technol. 57, 827–838.
Paipetis, A., Vlattas, C., Galiotis, C., 1996. Remote laser raman microscopy (reram): 1. Design and testing of a confocal microprobe. J. Raman Spectrosc. 27, 519–526.
Piggott, M.R., 1978. Expressions governing stress–strain curves in short fibre reinforced polymers. J. Mater. Sci. 13, 1709–1716.
Piggott, M.R., 1997. Why interface testing by single-fibre methods can be misleading. Compos. Sci. Technol. 57, 965–974.
Piggott, M.R., Harris, B., 1980. Compression strength of carbon glass and kevlar-49 fibre reinforced polyester resins. J. Mater. Sci. 15, 2523–2538.
Rosen, B.W., 1964. Tensile failure of fibrous composites. AIAA J. 2 (11), 1985–1991.
Rosen, B.W., 1965. Mechanics of composite strengthening. In: Fiber Composite Materials. American Society of Metals, Metals Park, Ohio, pp. 37–75.
Schapery, R.A., 1995. Prediction of compressive strength and kink bands in composites using a work potential. Int. J. Solids Struct. 32, 739–765.
Soutis, C., Curtis, P.T., 2000. A method for predicting the fracture toughness of cfrp laminates failing by fibre microbuckling. Composites Part A 31, 733–740.
Soutis, C., Smith, F.C., Matthews, F.L., 2000. Predicting the compressive engineering performance of carbon fibre-reinforced plastics. Composites Part A 31, 531–536.
van den Heuvel, P.W.J., Peijs, T., Young, R.J., 1997. Failure phenomena in two-dimensional multi-fibre microcomposites: 2. A Raman spectroscopic study of the influence of inter-fibre spacing on stress concentrations. Compos. Sci. Technol. 57, 899–911.
van-den-Heuvel, P.W.J., Peijs, T., Young, R.J., 1998. Failure phenomena in two-dimensional multi-fibre microcomposites: 3. A Raman spectroscopy study of the influence of interfacial debonding on stress concentrations. Compos. Sci. Technol. 58, 933–944.
Vincon, I., Allix, O., Sigety, P., Auvray, M.H., 1998. Compressive performance of carbon fibres: Experiment and analysis. Compos. Sci. Technol. 58, 1649–1658.
Vlattas, C., Galiotis, C., 1993. Deformation behaviour of liquid crystal polymer fibres: 1. Converting spectroscopic data into mechanical stress–strain curves in tension and compression. Polymer 35 (11), 2335–2347.
Vogler, T.J., Kyriakides, S., 1999. On the axial propagation of kink bands in fiber composites: Part I Experiments. Int. J. Solids Stuct. 36, 557–574.
Wood, J.R., Huang, Y., Young, R.J., Marom, G., 1995. Measurement of thermal strains during compressive fragmentation in single-fibre composites by Raman spectroscopy. Compos. Sci. Technol. 55, 223–229.
Wood, J.R., Wagner, H.D., Marom, G., 1994. A model for compressive fragmentation. Adv. Compos. Lett. 3, 133–138.